Diagnostic Accuracy of Virtual ^{18}F-FDG PET/CT Bronchoscopy for the Detection of Lymph Node Metastases in Non–Small Cell Lung Cancer Patients

Michael Herbrik[1], Jon Treffert[2], Bernhard Geiger[3], Carolin Riegger[1,4], Verena Hartung[5], Sandra Julia Rosenbaum-Krumme[5], Michael Forsting[1], Gerald Antoch[4], and Till A. Heusner[4]

[1]Departments of Diagnostic and Interventional Radiology and Neuroradiology, University Hospital Essen, University of Duisburg-Essen, Essen, Germany; [2]Siemens Health Care, Molecular Imaging, Knoxville, Tennessee; [3]Siemens Corporate Research, Princeton, New Jersey; [4]Univ. Dusseldorf, Medical Faculty, Department of Diagnostic and Interventional Radiology, D-40225 Dusseldorf, Germany; and [5]Department of Nuclear Medicine, University Hospital Essen, University of Duisburg-Essen, Essen, Germany

The aim of this study was to determine the diagnostic accuracy of ^{18}F-FDG PET/CT bronchoscopy for the detection of regional lymph node metastases in non–small cell lung cancer (NSCLC) patients; potential differences in the maximum standardized uptake value (SUVmax), mean SUV (SUVmean), short-axis diameter, and distance to the airways when comparing true-positive (TP), false-positive (FP), true-negative (TN), and false-negative (FN) lymph nodes; the smallest bronchus diameter accessible by virtual bronchoscopy; and the duration from the start of the virtual ^{18}F-FDG PET/CT bronchoscopy viewing tool until the images were displayed. **Methods:** Sixty-one consecutive NSCLC patients (mean age ± SD, 58 ± 10 y) underwent whole-body ^{18}F-FDG PET/CT. From these data, virtual ^{18}F-FDG PET/CT bronchoscopies were reconstructed. The duration from the start of the tool until the display of virtual bronchoscopy images was determined. The diagnostic accuracy of ^{18}F-FDG PET/CT bronchoscopy for the detection of regional lymph node metastases was evaluated on a lesion basis. Axial ^{18}F-FDG PET/CT scans served as the standard of reference. The SUVmax, SUVmean, short-axis diameter, and distance to the airways of regional lymph nodes were measured. Lymph nodes were classified as TP, FP, TN, and FN. The smallest bronchus diameter accessible by ^{18}F-FDG PET/CT bronchoscopy was measured. **Results:** The sensitivity, specificity, positive predictive value, negative predictive value, and accuracy of virtual ^{18}F-FDG PET/CT bronchoscopy for the detection of lymph node metastases were 76%, 87%, 85%, 79%, and 81%, respectively. The differences between the SUVmax, SUVmean, short-axis diameter, and distance to the airways of TP and FP as well as TN and FN lymph nodes were statistically significant ($P < 0.05$). The mean smallest diameter of accessible bronchi by ^{18}F-FDG PET/CT bronchoscopy was 3 mm. The mean time duration from the start of the virtual ^{18}F-FDG PET/CT bronchoscopy tool until the display of the images was 22 ± 7 s. **Conclusion:** Virtual fly-through 3-dimensional ^{18}F-FDG PET/CT bronchoscopy yields a high diagnostic accuracy for the detection of regional lymph node metastases and has access to bronchi even in the periphery of the lung. High SUVmax, high SUVmean, large small-axis diameter, and short distance to the airways aid detection of lymph node metastases with ^{18}F-FDG PET/CT bronchoscopy.

Key Words: virtual bronchoscopy; ^{18}F-FDG; PET/CT; bronchial carcinoma; lung cancer; non–small cell lung cancer

J Nucl Med 2011; 52:1520–1525
DOI: 10.2967/jnumed.111.092593

Lung and bronchus cancer represent the cancer types with the most cancer-related deaths in the United States, both in female and in male patients; with more than 220,000 newly diagnosed cases, it again was the most common newly diagnosed cancer type in the United States in 2010 (*1,2*). Non–small cell lung cancer (NSCLC) accounts for approximately 80% of all lung cancer disease. The choice of therapeutic options—surgery, radiation therapy, or chemotherapy alone or in combination with other treatment modalities—is based on the tumor stage (*3*). For a stage-adapted therapy, and thus an individual therapeutic concept, ^{18}F-FDG PET/CT clearly outperforms other imaging modalities with its high diagnostic accuracy for the detection of the primary bronchial carcinoma and metastases (*4,5*). The accurate determination of the pretherapeutic lymph node status in NSCLC patients is crucial for adequate therapy planning and for the patient's prognosis. On the basis of accurate staging of mediastinal lymph nodes and the detection of unsuspected distant metastases using ^{18}F-FDG PET/CT, compared with staging procedures based on other modalities, the rate of futile surgical procedures and the number of mediastinoscopies were significantly reduced (*6,7*).

Currently available PET/CT scanners contain a multislice, multidetector CT component and are capable of providing high-resolution CT and PET datasets that make it possible not only to generate and assess conventional PET/CT perspectives but also to generate virtual ^{18}F-FDG PET/CT bronchoscopy views and fly through the trachea and the bronchus tree, with functional information provided in the

Received May 16, 2011; revision accepted Jul. 29, 2011.
For correspondence or reprints contact: Till A. Heusner, University of Dusseldorf, Department of Radiology, Moorenstrasse 5, D-40225 Dusseldorf, Germany.
E-mail: Heusner@med.uni-duesseldorf.de
Published online Sep. 9, 2011.

same session. However, virtual ^{18}F-FDG PET/CT bronchoscopy until now was described only in some pilot, mostly feasibility-proving projects, whereas its diagnostic accuracy remains unknown (*8–11*).

To further investigate the possibilities of combined, virtual ^{18}F-FDG PET/CT bronchoscopy and to introduce this method into a more clinical context, the goal of this study was to determine the diagnostic accuracy of virtual ^{18}F-FDG PET/CT bronchoscopy for the detection of lymph node metastases in NSCLC patients.

MATERIALS AND METHODS

Patients

For staging purposes, 61 consecutive patients (mean age at time of investigation, 58 y; range, 36–80 y; SD, 10 y; sex, 37 men and 24 women) with histopathologically proven NSCLC were referred to whole-body ^{18}F-FDG PET/CT between July 2009 and August 2010 after optical bronchoscopy. All investigations were performed in a university hospital setting as part of the clinically indicated tumor-staging algorithm. Table 1 provides a detailed overview of the Union for International Cancer Control stage according to the reference standard. All patients signed an informed consent document that detailed the use of intravenous ^{18}F-FDG, CT contrast material, and rare potential side effects. No patient underwent anticancer treatment before or at the time of imaging. This retrospective study was performed in accordance with the regulations of the local ethics committee.

Whole-Body ^{18}F-FDG PET/CT

Whole-body ^{18}F-FDG PET/CT scans were obtained on a Biograph mCT hybrid PET/CT scanner (Siemens AG, Siemens Healthcare, Erlangen, Germany). The system consisted of a full-ring dedicated PET scanner, equipped with lutetium oxyorthosilicate crystals with an axial field of view of 21.8 cm, and a 2 × 64 slice spiral CT scanner.

Patients fasted for at least 6 h before intravenous application of ^{18}F-FDG (290 ± 50 MBq). Before the injection of the radioactive tracer, a blood sample was taken to ensure blood glucose levels were below 150 mg/dL. A water-based oral contrast agent (1,000 mL) was applied for bowel marking (*12*) within the ^{18}F-FDG uptake time. ^{18}F-FDG PET/CT started 60 min after the intravenous application of ^{18}F-FDG, beginning with the CT scan. CT data were acquired in the caudocranial direction, covering a field of view from the skull base to the upper thighs. Images were acquired at 120 kV, with automatic mA/s adjustment (Care Dose 4D [Siemens Molecular Imaging]; Care Dose preset, 210 mAs). An iodinated contrast agent (100 mL) (Ultravist 300; Schering AG, Berlin, Germany) was administered with an automated dual-head injector (Medrad Stellant; Medizinische Systeme GmbH, Volkach, Germany), with a flow rate of 2 mL/s, followed by a flush of 2.5 mL of saline/s.

TABLE 1
Number of Patients and T Stage

T stage	Patients (*n*)
IB	3
IIA	2
IIB	2
IIIA	18
IIIB	20
IV	16

The start delay was set to 70 s. The images were acquired with 5-mm slice thickness, a 5-mm increment, and a pitch of 1. Images were reconstructed to 1.5-mm slice thickness. The rotation time of the CT tube was 0.5 s. CT data were acquired in slight expiration. After the acquisition of the CT data, PET images were obtained in 3-dimensional mode in the same position as the CT images.

The PET emission time was set to 2 min per bed position (overlap per bed position, 45%). PET images were reconstructed according to the ordered-subsets expectation maximization algorithm using 4 iterations and 8 subsets. A 3-dimensional gaussian filter of 4.0 mm in full width at half maximum was applied.

Virtual ^{18}F-FDG PET/CT Bronchoscopy

An investigational software application has been developed that extends conventional (CT-only) virtual endoscopy (bronchoscopy or colonoscopy) by the simultaneous display of coregistered PET information. After the automated segmentation of the airway, the user is provided with fused multiplanar reconstruction views (sagittal, coronal, and transaxial) and a virtual endoscopic view of the data (Figs. 1 and 2). The user can optionally swap one of the multiplanar reconstruction views with a volume rendering of the segmented airway tree. A PET activity overlay is provided in the endoscopic view. A perspective raycaster is used to determine the endoluminal surface.

PET-specific activity (normalized to standardized uptake value [SUV]) is determined at the surface. Local color components of the anatomic surface rendering are modified when the PET activity exceeds a user-adjustable threshold. The color modification is proportional to the PET activity; it is not a quantitative display but serves primarily to alert the user to the presence of surface PET activity exceeding the SUV threshold.

An intuitive fly-through interface provides navigation of the airways within the virtual endoscopic view. The endoscope path can be displayed on the planar views. When the user selects a point on the surface in endoscopic view, and during endoscopic navigation, the planar views are adjusted so that the current endoscope position is visible with a line graphic indicating the endoscope orientation. Navigation sessions can be saved directly to a video file.

Reference Standard

Because the goal of our study was to assess the diagnostic accuracy of virtual ^{18}F-FDG PET/CT bronchoscopy for the detection of thoracic lymph node metastases, compared with the axial FDG PET/CT, the findings of the axial ^{18}F-FDG PET/CT scans were used as the reference standard for the evaluation.

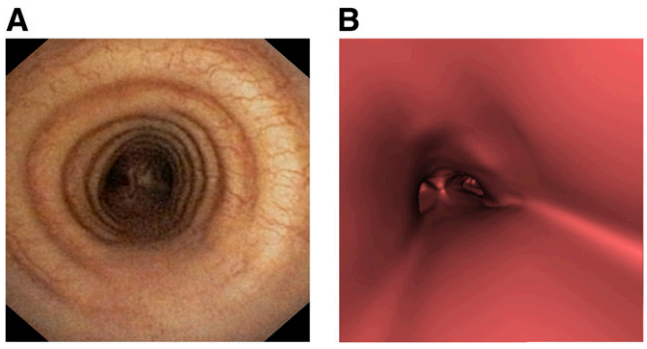

FIGURE 1. Optical bronchoscopy (A) of 55-y-old man with histopathologically proven, metastasized NSCLC (TNM stage, T2N3M0) without suggestions of malignancy on optical bronchoscopy. Also on CT bronchoscopy (B), there is no (morphologic) sign of malignancy.

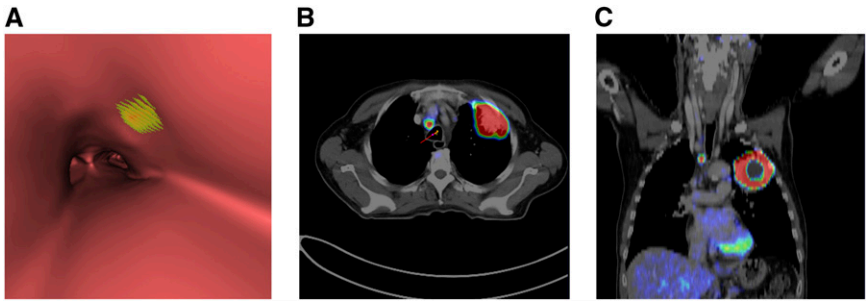

FIGURE 2. With addition of ^{18}F-FDG PET information to 3-dimensional virtual ^{18}F-FDG PET/CT bronchoscopy (A), lymph node metastasis (SUVmax, 17.1) becomes visible in position 2R (yellow dot on tracheal surface), as confirmed on axial (B) and coronal (C) ^{18}F-FDG PET/CT.

Axial ^{18}F-FDG PET/CT Evaluation

Two board-certified radiologists and 1 nuclear medicine physician (all with more than 5 y of PET/CT experience) evaluated the images. Decisions were made in consensus. On a first digital workstation, the axial ^{18}F-FDG PET/CT scans were reviewed using a TrueD Workstation (Siemens Medical Solutions, Erlangen, Germany) connected to a PACS workstation.

Mediastinal, hilar, interlobar, and lobar lymph nodes were evaluated by reference to the classification by Mountain and Dresler (*13*). Images were analyzed as follows: all lymph nodes detectable on CT were included in the analysis. These lymph nodes were evaluated for any focally increased PET signal. PET foci in lymph nodes indicated metastases. A nonelevated PET signal or a signal considered compatible with physiologic lymphatic uptake was rated negative. Lymph node size did not directly affect PET/CT interpretation but was indirectly considered with respect to the intensity of the PET signal. In short, a given PET focus was rated positive in a small lymph node rather than in a large lymph node, accounting for partial-volume effects. The decision was an empiric one based on the long-term imaging experience of the 3 readers. Quantitative measurements such as SUVs on PET were done in a concomitant manner but were not used for final decision making (*14*). The following parameters were documented: for thoracic lymph nodes—localization according to Mountain and Dresler (*13*), short-axis diameter (measured orthogonally to the longest axial diameter) (mm), shortest distance to the airways (trachea, bronchi) (mm), maximum SUV (SUVmax), mean SUV (SUVmean), and dichotomous differentiation into metastases and physiologic nodes—and for bronchi—smallest diameter of accessible bronchi in the periphery of the lung (mm).

Virtual ^{18}F-FDG PET/CT Bronchoscopy Evaluation

The investigational PET/CT virtual endoscopy application was installed on a Syngo Multimodality Workplace (Siemens Health Care). The first step of the evaluation was to level the PET window of the virtual bronchoscopy tool.

Investigators, in consideration of the simultaneously visible ^{18}F-FDG PET/CT images in the 3 orthogonal planes, virtually flew through the airways while leveling the PET device (Fig. 2). A lesion-based analysis was done by dividing lesions into true-positives (TPs), true-negatives (TNs), false-positives (FPs), and false-negatives (FNs).

The line of vision from the tip of the virtual scope was controlled on cross-sectional images (Fig. 3).

Statistical Analysis

The duration from the start of the virtual ^{18}F-FDG PET/CT bronchoscopy tool until display of all images was measured. The mean, minimum, maximum, and SD of the SUVmax, SUVmean, distances to the airways of the lymph nodes, and their short-axis diameters were calculated for TP, FP, TN, and FN lesions. The following parameters were determined on a lesion basis: sensitivity, specificity, positive predictive value, negative predictive value, and accuracy of the virtual ^{18}F-FDG PET/CT bronchoscopy tool for the detection of lymph node metastases. Differences between the measurements of TP and FP lymph nodes and TN and FN lymph nodes were tested for statistical significance using the Mann–Whitney Wilcoxon test, using a significance level of $P = 0.05$. The smallest bronchus diameter accessible by virtual ^{18}F-FDG PET/CT bronchoscopy was measured.

RESULTS

Whole-Body ^{18}F-FDG PET/CT

Patient Population and Tumor Characterization. In 28 patients, the primary NSCLC was localized centrally, and in 33 patients peripherally. The left upper lobe was affected 19 times, left lower lobe 5 times, right upper lobe 21 times, right lower lobe 10 times, and middle lobe 6 times. All diagnoses were verified histopathologically. The mean largest diameter was 44 mm (range, 11–118 mm; SD, 21.2 mm). The mean SUVmax was 13.2 (range, 1.3–35.6; SD, 7.0); the mean SUVmean was 5.8 (range, 1.1–18.9; SD, 3.0).

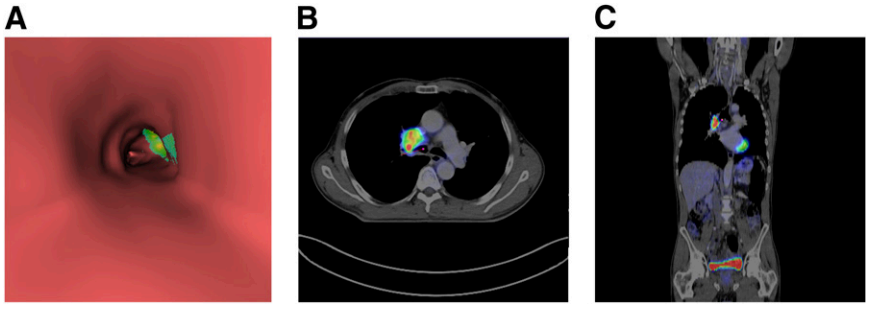

FIGURE 3. Axial (B) and coronal (C) ^{18}F-FDG PET/CT and virtual ^{18}F-FDG PET/CT bronchoscopy (A) of 73-y-old man with histopathologically proven NSCLC. Cross-sectional image shows virtual view direction by red or yellow line in axial and coronal views; tip of virtual scope is marked with purple dot. View is directed at bifurcation of right main bronchus. In virtual ^{18}F-FDG PET/CT bronchoscopy view, primary NSCLC lesion is marked as green or yellow area.

TABLE 2
Localization of Investigated Lymph Nodes According to Classification of Mountain and Dresler (*13*)

Nodal station	Lymph nodes (*n*)	Patients (*n*)
1	68	37
2	81	39
3	3	3
4	74	42
5	15	7
6	27	20
7	58	49
8	4	4
10	89	52
11	39	24
12	4	3

Lymph Nodes. Overall, 462 mediastinal, hilar, interlobar, and lobar lymph nodes with a minimum short-axis diameter of 3 mm were evaluated. The mean number of lymph nodes evaluated per patient was 8 (range, 2–19 lymph nodes; SD, 3.7). Table 2 provides a summary of lymph node localization.

The mean short-axis diameter of all nodes ($n = 462$) was 11 mm (range, 3–74 mm; SD, 6.9 mm), and the mean short-axis diameter of lymph node metastases ($n = 222$) was 14 mm (range, 5–74 mm; SD, 8.3 mm). The mean short-axis diameter of physiologic nodes ($n = 240$) was 8 mm (range, 3–25 mm; SD, 2.9 mm). The mean shortest distance to the tracheal or bronchial surface of all evaluated lymph nodes was 6 mm (range, 1–44 mm; SD, 9.1 mm), and the mean shortest distance of lymph node metastases to the tracheal or bronchial surface was 6 mm (range, 1–44 mm; SD, 8.3 mm). The mean shortest distance of physiologic lymph nodes to the tracheal or bronchial surface was 7 mm (range, 1–43 mm; SD, 9.8 mm).

The mean SUVmax of all evaluated lymph nodes was 4.5 (range, 0.6–23.1; SD, 3.8), and the mean SUVmax of lymph node metastases was 6.8 (range, 2.7–23.1; SD, 4.1). The mean SUVmax of physiologic lymph nodes was 2.1 (range, 0.6–5.5; SD, 0.7).

The mean SUVmean of all evaluated lymph nodes was 3.1 (range, 2.5–14.8; SD, 2.1), and the mean SUVmean of metastatic lymph nodes was 4.4 (range, 1.6–14.8; SD, 2.3). The mean SUVmean of physiologic lymph nodes was 1.7 (range, 0.3–4.5; SD, 0.6).

Virtual ^{18}F-FDG PET/CT Bronchoscopy

Duration of ^{18}F-FDG PET/CT Bronchoscopy Tool-Starting Process. The mean duration between the start of the virtual ^{18}F-FDG PET/CT bronchoscopy software tool until display of the virtual ^{18}F-FDG PET/CT bronchoscopy images was 22 s (range, 7–74 s; SD, 18 s).

Lymph Nodes. According to the whole-body ^{18}F-FDG PET/CT, standard virtual ^{18}F-FDG PET/CT bronchoscopy was TP in 170 lymph nodes, TN in 207, FP in 32, and FN in 53 (Figs. 4 and 5). Therefore, the sensitivity, specificity, positive predictive value, negative predictive value, and accuracy of virtual ^{18}F-FDG PET/CT bronchoscopy for the detection of lymph node metastases were 76%, 87%, 85%, 79%, and 81%, respectively.

The difference between the short-axis diameter of TP and FP lymph nodes and TN and FN lymph nodes was statistically significant ($P < 0.001$).

The difference between the shortest distance to the airways of TP and FP lymph nodes was not statistically significant ($P = 0.41$), whereas the difference between the shortest distance to the airways of TN and FN lymph nodes was statistically significant ($P = 0.01$).

The difference between the SUVmax of TP and FP lymph nodes, like the difference between the SUVmax of TN and FN lymph nodes, was statistically significant ($P < 0.001$).

The difference between the SUVmean of TP and FP lymph nodes was statistically significant ($P < 0.001$).

The difference between the SUVmean of TN lymph nodes (mean, 1.7; range, 0.5–4.5; SD, 0.6) and FN lymph nodes (mean, 3.2; range, 1.6–8; SD, 1.4) was also statistically significant ($P < 0.001$).

Table 3 provides a detailed overview of TP, FP, TN and FN lymph nodes.

Bronchi. The mean smallest diameter of accessible bronchi in the periphery of the lung by virtual fly-through bronchoscopy was 3.2 mm (range, 2–6.1 mm; SD, 0.7 mm).

DISCUSSION

Virtual 3-dimensional ^{18}F-FDG PET/CT visualizations such as virtual bronchoscopies, mediastinoscopies, or colonographies are technically feasible by image postprocessing using current high-resolution PET and CT data (*8–11, 15,16*). The short durations (seconds) from the start of the tool to the display of the virtual ^{18}F-FDG PET/CT bronchoscopy datasets are clearly operational in clinical routine.

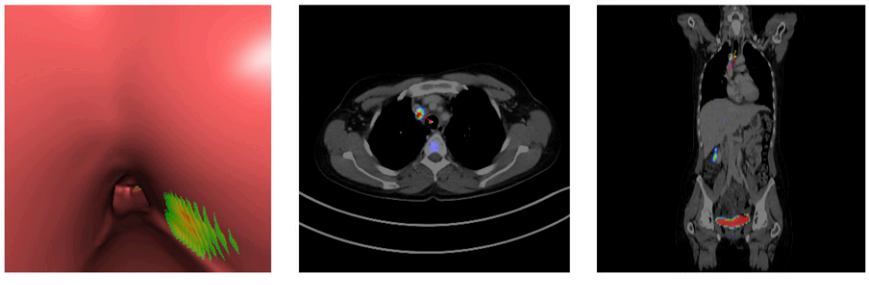

FIGURE 4. ^{18}F-FDG PET–positive lymph node metastasis (SUVmax, 12.3) adjacent to surface of right wall of trachea that was TP on virtual ^{18}F-FDG PET/CT bronchoscopy (A) in 76-y-old man patient with stage IIA disease. Axial (B) and coronal (C) ^{18}F-FDG PET/CT confirm presence of metastasis.

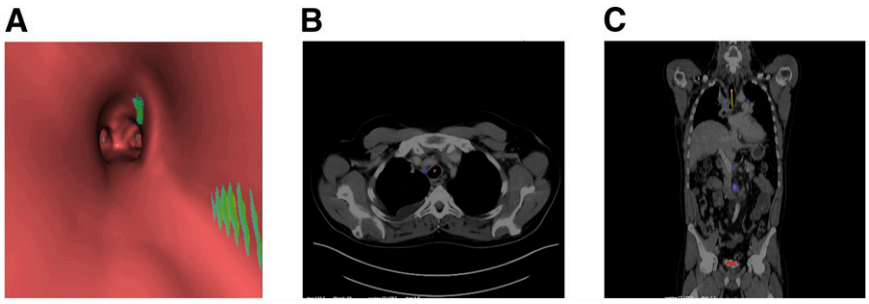

FIGURE 5. FP lesion with apparent focal PET uptake in positions 2R and 4R on virtual ^{18}F-FDG PET/CT bronchoscopy (A). On axial (B) and coronal (C) ^{18}F-FDG PET/CT, there was no corresponding lesion with elevated uptake was detectable.

Virtual ^{18}F-FDG PET/CT bronchoscopy enables noninvasive fly-through, even in relatively small airways in the periphery of the lung, and the detection of PET-positive lymph node metastases adjacent to airway structures, with a high diagnostic accuracy. Virtual ^{18}F-FDG PET/CT bronchoscopy represents a technique that not only images surface morphologic features of central and peripheral airways but also displays functional information underneath the wall of the trachea and bronchi. With this complementary added information, compared with morphologic data alone, the paratracheal and parabronchial lymph node metastases become visible. Virtual ^{18}F-FDG PET/CT may become an important preprocedural tool to better localize affected lymph nodes, especially before endobronchial ultrasound–guided biopsy of paratracheal or parabronchial lymph nodes.

For transbronchial, fiberoptic–bronchoscopically guided biopsies, especially in small tumors without morphologic signs such as bronchus invasion, compression, or bronchial irregularities, PET/CT bronchoscopy may be a valuable planning tool (*8*). Virtual ^{18}F-FDG PET/CT bronchoscopy does not add any radiation exposure to the exposure caused by ^{18}F-FDG PET/CT because bonchoscopy datasets can be reconstructed from the PET/CT images.

Further technical developments seem to be desirable to enhance the features of this tool: a software tool that offers variance in visualization of the transparency of the airway wall may not only help the visualization of functional data of tumor tissue adjacent to the airway surface but also help the direct visualization of the malignancy. A more or less transparent tracheal and bronchial wall could allow the assessment of the configuration of the lesion and distances between surface and malignant lesions, which may affect biopsy strategy. Because this option is not yet available, a side-by-side evaluation of PET/CT bronchoscopy with cross-sectional PET/CT images is required.

Another goal of future technical developments will be the implementation of a more sophisticated PET displaying algorithm. With the current software version in use, we found several FP lesions adjacent to the bronchus surface, most likely resulting from physiologic uptake by airway walls and a shine-through effect from adjacent physiologic mediastinal structures such as vessels (blood pool) or lymph nodes not affected by tumor. In addition, FN results occur in lymph nodes that are localized relatively far from the surface (~12 mm). Adapting the software algorithm in use may reduce the number of FN lesions in the future. The next clinical study step will be to evaluate whether preinterventional virtual ^{18}F-FDG PET/CT bronchoscopies ease fiberoptically guided biopsies and endobronchial ultrasound (EBUS)–guided biopsies.

This study has some limitations. Histopathology would have provided the better reference standard but was not available in all patients. Micrometastases cannot be detected with any imaging procedure, and FP findings occur with PET/CT when defining lymph node metastases. Thus, histopathology would have been desirable. However, because PET/CT has a relatively high accuracy for the detection of lymph node metastases in NSCLC, using PET/CT data as the standard of reference may be acceptable (*6*). Considering this gold standard, the calculated diagnostic accuracy of virtual ^{18}F-FDG PET/CT bronchoscopy may have been overestimated (as compared with a gold standard histopathology). Thus, the true accuracy of virtual ^{18}F-FDG PET/CT may prove to be lower than 81% when assessed

TABLE 3
Characteristics of Investigated Lymph Nodes

Characteristic	TP (n = 170)		FP (n = 32)		TN (n = 207)		FN (n = 53)	
	Mean ± SD	Range	Mean ± SD	Range	Mean ± SD	Range	Mean ± SD	Range
Short-axis diameter (mm)	14.4 ± 9	5–74*	6.5 ± 2.1	3–10	7.8 ± 3.0	3–25	11.8 ± 4.7	5–24
Shortest distance of lymph nodes to adjacent airways (mm)	4.7 ± 6.7	1–35	4.5 ± 6.9	2–36	7.1 ± 10.1	1–43	10.1 ± 11.3	1–44
SUVmax	7.3 ± 4.1	2.3–23.1	2.4 ± 0.4	1.4–3.5	2.2 ± 1.0	0.6–12	5.3 ± 3.7	2.1–17.8
SUVmean	4.7 ± 2.4	1.6–14.8	1.9 ± 0.5	0.3–2.8	1.7 ± 0.6	0.5–4.5	3.2 ± 1.4	1.6–8.0

*Marks statistically significant differences.

prospectively with histopathology as a reference standard. Bearing this in mind, virtual ^{18}F-FDG PET/CT bronchoscopy and EBUS may be of comparable diagnostic accuracy for the detection of lymph node metastases, with accuracies for EBUS reported to be 57%–93% in the literature (*17–19*). The true accuracy will have to be assessed in future prospective trials.

Another limitation is the manual PET thresholding in virtual ^{18}F-FDG PET/CT bronchoscopy, which is based on correlation with axial ^{18}F-FDG PET/CT data. Though this adjustment has to be done in the evaluation of normal axial ^{18}F-FDG PET/CT scans also, in the virtual bronchoscopy view, there are no qualitative reference points for windowing/thresholding the PET image because no structure below the surface is visible. Thus, axial PET/CT data are required for correlation when thresholds are applied to the bronchoscopy datasets. It is noticeable that most FP lymph nodes are localized in positions 2 and 10 (*13*), possibly a result of several structures—such as the aorta and hilum—with physiologically elevated ^{18}F-FDG uptake adjacent to these positions. In the future, this problem may be solved by adjusting the display algorithm to the expected surrounding physiologic PET activity.

CONCLUSION

Virtual 3-dimensional ^{18}F-FDG PET/CT bronchoscopy yields a relatively high diagnostic accuracy for the detection of mediastinal lymph node metastases that is at least comparable to that of EBUS. In the future, virtual ^{18}F-FDG PET/CT bronchoscopy may be used for endoscopically guided biopsy planning.

DISCLOSURE STATEMENT

The costs of publication of this article were defrayed in part by the payment of page charges. Therefore, and solely to indicate this fact, this article is hereby marked "advertisement" in accordance with 18 USC section 1734.

ACKNOWLEDGMENT

No potential conflict of interest relevant to this article was reported.

REFERENCES

1. Jemal A, Siegel R, Xu J, Ward E. Cancer statistics 2010. *CA Cancer J Clin.* 2010;60:277–300.
2. Jemal A, Siegel R, Ward E, Hao Y, Xu J, Thun MJ. Cancer statistics, 2009. *CA Cancer J Clin.* 2009;59:225–249.
3. Freudenberg LS, Rosenbaum SJ, Beyer T, Bockisch A, Antoch G. PET versus PET/CT dual-modality imaging in evaluation of lung cancer. *Radiol Clin North Am.* 2007;45:639–644.
4. Kligerman S, Digumarthy S. Staging of non-small cell lung cancer using integrated PET/CT. *AJR.* 2009;193:1203–1211.
5. Antoch G, Stattaus J, Nemat AT, et al. Non-small cell lung cancer: dual-modality PET/CT in preoperative staging. *Radiology.* 2003;229:526–533.
6. van Tinteren H, Hoekstra OS, Smit EF, et al. Effectiveness of positron emission tomography in the preoperative assessment of patients with suspected non-small-cell lung cancer: the PLUS multicentre randomised trial. *Lancet.* 2002;359:1388–1393.
7. Herder GJ, Kramer H, Hoekstra OS, et al. Traditional versus up-front [^{18}F] fluorodeoxyglucose-positron emission tomography staging of non-small-cell lung cancer: a Dutch cooperative randomized study. *J Clin Oncol.* 2006;24:1800–1806.
8. Englmeier KH, Seemann MD. Multimodal virtual bronchoscopy using PET/CT images. *Comput Aided Surg.* 2008;13:106–113.
9. Quon A, Napel S, Beaulieu CF, Gambhir SS. "Flying through" and "flying around" a PET/CT scan: pilot study and development of 3D integrated ^{18}F-FDG PET/CT for virtual bronchoscopy and colonoscopy. *J Nucl Med.* 2006;47:1081–1087.
10. Seemann MD, Schaefer JF, Englmeier KH. Virtual positron emission tomography/computed tomography-bronchoscopy: possibilities, advantages and limitations of clinical application. *Eur Radiol.* 2007;17:709–715.
11. Yerushalmi D, Mullick R, Quon A, et al. Simulations of virtual PET/CT 3-D bronchoscopy imaging using a physical porcine lung-heart phantom. *Mol Imaging Biol.* 2009;11:275–282.
12. Antoch G, Kuehl H, Kanja J, et al. Dual-modality PET/CT scanning with negative oral contrast agent to avoid artifacts: introduction and evaluation. *Radiology.* 2004;230:879–885.
13. Mountain CF, Dresler CM. Regional lymph node classification for lung cancer staging. *Chest.* 1997;111:1718–1723.
14. Heusner TA, Kuemmel S, Hahn S, et al. Diagnostic value of full-dose FDG PET/CT for axillary lymph node staging in breast cancer patients. *Eur J Nucl Med Mol Imaging.* 2009;36:1543–1550.
15. Veit-Haibach P, Kuehle CA, Beyer T, et al. Diagnostic accuracy of colorectal cancer staging with whole-body PET/CT colonography. *JAMA.* 2006;296:2590–2600.
16. Itano H, Hirokawa Y, Takauchi K. Clinical utility of three-dimensional integrated 18F-fluorodeoxyglucose positron-emission tomography/computed tomography virtual mediastinoscopy. *Interact Cardiovasc Thorac Surg.* 2010;10:981–985.
17. Cerfolio RJ, Bryant AS, Eloubeidi MA, et al. The true false negative rates of esophageal and endobronchial ultrasound in the staging of mediastinal lymph nodes in patients with non-small cell lung cancer. *Ann Thorac Surg.* 2010;90:427–434.
18. Szlubowski A, Kuzdzał J, Kołodziej M, et al. Endobronchial ultrasound-guided needle aspiration in the non-small cell lung cancer staging. *Eur J Cardiothorac Surg.* 2009;35:332–335, discussion 335–336.
19. Rintoul RC, Skwarski KM, Murchison JT, Wallace WA, Walker WS, Penman ID. Endobronchial and endoscopic ultrasound-guided real-time fine-needle aspiration for mediastinal staging. *Eur Respir J.* 2005;25:416–421.

JNM The Journal of NUCLEAR MEDICINE

Diagnostic Accuracy of Virtual ^{18}F-FDG PET/CT Bronchoscopy for the Detection of Lymph Node Metastases in Non–Small Cell Lung Cancer Patients

Michael Herbrik, Jon Treffert, Bernhard Geiger, Carolin Riegger, Verena Hartung, Sandra Julia Rosenbaum-Krumme, Michael Forsting, Gerald Antoch and Till A. Heusner

J Nucl Med. 2011;52:1520-1525.
Published online: September 9, 2011.
Doi: 10.2967/jnumed.111.092593

The Journal of Nuclear Medicine is published monthly.
SNMMI | Society of Nuclear Medicine and Molecular Imaging
1850 Samuel Morse Drive, Reston, VA 20190.
(Print ISSN: 0161-5505, Online ISSN: 2159-662X)

SNMMI SOCIETY OF NUCLEAR MEDICINE AND MOLECULAR IMAGING